*Leukemia & Lymphoma*, 2014; Early Online: 1–2

ISSN: 1042-8194 print / 1029-2403 online
DOI: 10.3109/10428194.2014.966244

informa
healthcare

LETTER TO THE EDITOR

# The NOD/Shi-*scid*/IL-2Rγ$^{null}$ mice xenograft model recapitulates anaplastic large cell lymphoma dissemination to the bladder

Tomoo Daifu[1], Katsutsugu Umeda[1], Kagehiro Kouzuki[1], Takayuki Hamabata[1], Seishiro Noudomi[1], Satoshi Saida[1], Itaru Kato[1], Hidefumi Hiramatsu[1], Ken-ichiro Watanabe[1], Naoki Terada[2], Masaaki Imamura[2], Osamu Ogawa[2], Toshio Heike[1] & Souichi Adachi[3]

[1]*Department of Pediatrics,* [2]*Department of Urology and* [3]*Human Health Sciences, Graduate School of Medicine, Kyoto University, Kyoto, Japan*

Anaplastic large cell lymphoma (ALCL) is a T-cell lymphoma characterized by the proliferation of large pleomorphic CD30 + cells. Typical cases are associated with t(2;5)(p23;q35), which results in the production of a nucleophosmin (NPM)–anaplastic lymphoma kinase (ALK) fusion protein. More than 70% of patients with ALCL present with aggressive stage III or IV disease [1], and approximately 60% of cases of systemic ALCL involve extranodal sites such as the skin, bone, soft tissue, lung and liver [2]. There are a few reports of adult patients with dissemination to the bladder [3–6]; however, to the best of our knowledge, such a rare type of extranodal dissemination has not been reported in pediatric patients. Although the mechanism underlying extranodal dissemination of the disease remains unknown, appropriate xenograft models that recapitulate this dissemination would provide invaluable information. Here, we present a pediatric patient with systemic ALCL with bladder involvement, and report the successful establishment of a xenograft model of extranodal dissemination to the bladder.

A 10-year-old girl was admitted to our hospital with macroscopic hematuria. Abdominal ultrasonography, pelvic magnetic resonance imaging and $^{18}$F-fluorodeoxyglucose (FDG) positron emission tomography-computed tomography (CT) revealed a 3 cm tumor in the bladder, two small subcutaneous masses and hydronephrosis of the right kidney [Figures 1(A) and 1(B)], while lymphadenopathy and hepatosplenomegaly were not detected. Blood tests were normal, apart from a slight increase in soluble interleukin-2 receptor (IL-2R) levels (938 U/mL). Examination of a bone marrow aspirate and cerebrospinal fluid revealed no metastatic disease. Histological examination of a bladder biopsy specimen revealed monotonous infiltration by large lymphoid cells [Figure 1(E)], which were positive for CD4, CD25, CD30, granzyme B, epithelial membrane antigen and ALK [Figures 1(F) and 1(G) and data not shown]. Flow cytometry showed that the tumor cells were positive for CD4, CD7, CD8, CD25, CD30, human leukocyte antigen (HLA)-DR and cytoplasmic CD3. Polymerase chain reaction (PCR) detected clonal rearrangement of the T cell receptor (TCR) γ and β genes. A diagnosis of ALK-positive ALCL involving the bladder and subcutaneous tissue was made, and the patient was treated with six courses of multidrug chemotherapy according to the ALCL99 protocol [7]. All measurable lesions disappeared after two courses of chemotherapy. The patient was alive and in complete remission at 1 year and 9 months post-treatment.

To establish a xenograft model of ALCL, tumor cells were injected subcutaneously into the flanks of a NOD/Shi-*scid*/IL-2Rγ$^{null}$ (NOG) mouse [8], which was obtained from the Central Institute of Experimental Animals (Kawasaki, Japan). The tumor sample was collected from the patient (who provided written informed consent under the guidelines of the Kyoto University Graduate School and Faculty of Medicine Ethics Committee). Twelve weeks after transplant, the mouse was sacrificed, and the primary injection site and metastases were removed for histological or flow cytometric analysis. We found that the injection site, spleen and bladder had been engrafted with tumor cells [Figures 1(C) and 1(D)]. This was confirmed by hematoxylin and eosin staining and immunostaining for ALK and CD30 [Figures 1(H)–1(M)]. The histological findings resembled those observed in the patient's tissues [Figures 1(F) and 1(G)]. Furthermore, flow cytometry showed that the immunophenotype of the engrafted tumors was similar to that of the patient's tumor. In contrast, tumor involvement was not observed in other organs, such as the liver, kidney, lung, pancreas or subcutaneous tissue. Bone marrow involvement was not observed. Collectively, these data suggest that ALCL cells of the patient had intrinsic properties allowing metastasis to specific extranodal sites.

Although ALCL involves various extranodal organs, only four patients with bladder involvement have been reported

Correspondence: Katsutsugu Umeda, Department of Pediatrics, Graduate School of Medicine, Kyoto University, 54 Kawahara-cho, Shogoin, Sakyo-ku, Kyoto 606-8507, Japan. Tel: + 81-75-751-3290. Fax: + 81-75-752-2361. E-mail: umeume@kuhp.kyoto-u.ac.jp

*Received 16 July 2014; revised 6 September 2014; accepted 11 September 2014*

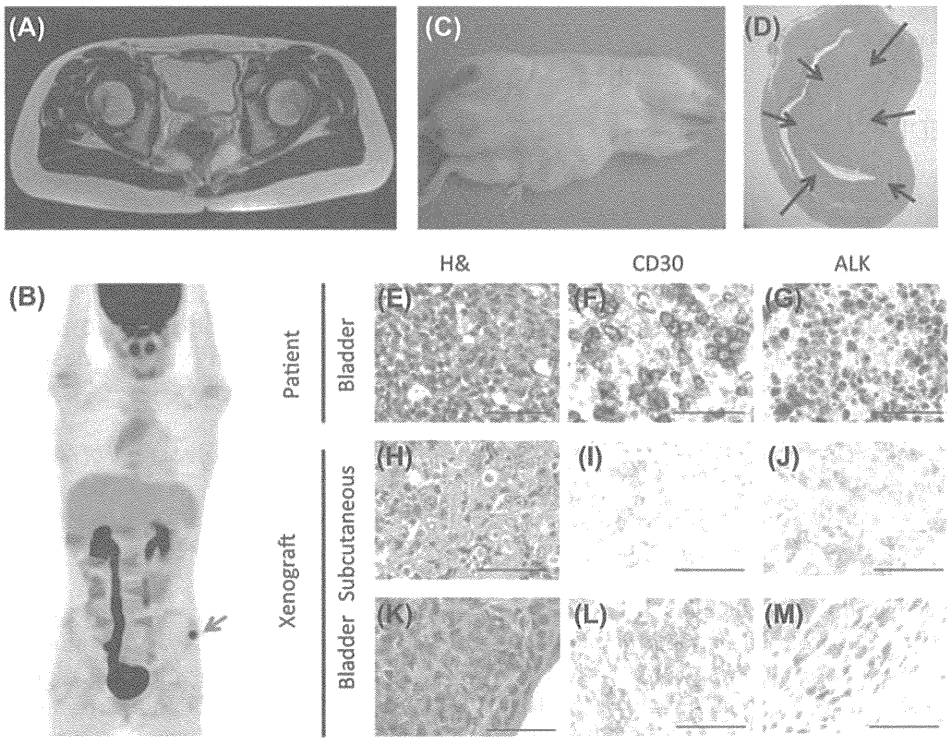


Figure 1. (A, B) Radiographic changes at diagnosis. Abdominal T2-weighted magnetic resonance imaging (A) and $^{18}$F-FDG positron emission tomography-CT (B) show the tumor in the bladder and subcutaneous tissue (arrow). Hydronephrosis of the right kidney was also observed (arrowheads). (C) Gross view of the engrafted subcutaneous tumor (arrow) in a NOG mouse at 12 weeks post-xenotransplant. (D) Hematoxylin and eosin staining of the engrafted tumor (arrows) in the bladder of a NOG mouse. (E-M) Staining of the bladder tumor in the patient and engrafted cells in the NOG mouse with hematoxylin and eosin (E, H, K), and with antibodies to CD30 antibody (F, I, L) and ALK (G, J, M). Scale bars = 50 $\mu$m.

to date [3–6]. Previous patients were all adult males, whereas our patient is the first reported pediatric case. The four adult patients showed diffuse lymphadenopathy, and extranodal involvement other than bladder was observed in only two adult patients. In contrast, our patient had extranodal involvement (bladder and subcutaneous tissues) without nodal sites. For all four patients whose clinical data were available, multi-drug chemotherapy was effective, leading to continuous complete remission.

Previous reports of a xenograft model of ALCL cell lines or clinical samples showed diffuse lymphadenopathy as well as extranodal dissemination to various organs; however, bladder involvement has not been reported [9,10]. In contrast, our xenotransplant model recapitulated dissemination to the bladder. One possible reason for the result is that our established immunodeficient NOG mouse showed significantly better human cell engraftment in extramedullary organs compared with other immunodeficient mice, possibly due to a complete lack of natural killer cell activity and dendritic cell dysfunction, as previously reported [8]. Alternatively, our patient showed a biological property distinct from other patients with ALCL, who did not show bladder dissemination. Thus, further studies are required to elucidate the mechanism underlying the extranodal dissemination of ALCL.

Nevertheless, the xenograft model reported herein faithfully recapitulated the extranodal dissemination of ALCL cells. Thus, it may serve as a useful experimental tool for analyzing the pathophysiology of disease progression and testing novel treatments of the disease.

***Potential conflict of interest:*** Disclosure forms provided by the authors are available with the full text of this article at www.informahealthcare.com/lal.

## References

[1] Stein H, Foss HD, Dürkop H, et al. CD30(+) anaplastic large cell lymphoma:a review of its histopathologic, genetic, and clinical features. Blood 2000;96:3681–3695.
[2] Falini B, Pileri S, Zinzani PL, et al. ALK+ lymphoma: clinico-pathological findings and outcome. Blood 1999;93:2697–2706.
[3] Pai SA, Naresh KN, Patil PU. Systemic anaplastic large cell lymphoma presenting as a bladder neoplasm. Leuk Lymphoma 2004;45:841–843.
[4] Murphy AJ, O'Neill P, O'Brien F, et al. Anaplastic large cell lymphoma: a unique presentation with urinary bladder involvement: a case report. Int J Surg Pathol 2005;13:369–373.
[5] Gómez-Román JJ, Cobo ML, Val-Bernal JF. Anaplastic lymphoma kinase-positive anaplastic large cell lymphoma presenting as a bladder neoplasm. Pathol Int 2008;58:249–252.
[6] Blick C, Abdelhadi S, Bailey D, et al. Anaplastic, T-cell, non-Hodgkin's Lymphoma presenting with haematuria. Sci World J 2008;8:342–345.
[7] Le Deley MC, Rosolen A, Williams DM, et al. Vinblastine in children and adolescents with high-risk anaplastic large-cell lymphoma: results of the randomized ALCL99-vinblastine trial. J Clin Oncol 2010;28:3987–3993.
[8] Ito M, Hiramatsu H, Kobayashi K, et al. NOD/SCID/gamma(c) (null) mouse: an excellent recipient mouse model for engraftment of human cells. Blood 2002;100:3175–3182.
[9] Pfeifer W, Levi E, Petrogiannis-Haliotis T, et al. A murine xenograft model for human CD30 + anaplastic large cell lymphomacell lymphoma. Successful growth inhibition with an anti-CD30 antibody (HeFi-1). Am J Pathol 1999;155:1353–1359.
[10] Zhang M, Yao Z, Zhang Z, et al. Effective therapy for a murine model of human anaplastic large-cell lymphoma with the anti-CD30 monoclonal antibody, HeFi-1, does not require activating Fc receptors. Blood 2006;108:705–710.

LIVER TRANSPLANTATION 20:1127–1137, 2014

ORIGINAL ARTICLE

# Hepatocytes Buried in the Cirrhotic Livers of Patients With Biliary Atresia Proliferate and Function in the Livers of Urokinase-Type Plasminogen Activator–NOG Mice

**Hiroshi Suemizu,[1]* Kazuaki Nakamura,[3]* Kenji Kawai,[2] Yuichiro Higuchi,[1] Mureo Kasahara,[4] Junichiro Fujimoto,[5] Akito Tanoue,[3] and Masato Nakamura[6]**

*[1]Biomedical Research Department, and [2]Pathology Research Department, Central Institute for Experimental Animals, Kanagawa, Japan; [3]Department of Pharmacology, [4]Department of Transplant Surgery, and [5]Clinical Research Center, National Center for Child Health and Development, Tokyo, Japan; and [6]Department of Pathology and Regenerative Medicine, Tokai University School of Medicine, Kanagawa, Japan*

The pathogenesis of biliary atresia (BA), which leads to end-stage cirrhosis in most patients, has been thought to inflame and obstruct the intrahepatic and extrahepatic bile ducts. BA is not believed to be caused by abnormalities in parenchymal hepatocytes. However, there has been no report of a detailed analysis of hepatocytes buried in the cirrhotic livers of patients with BA. Therefore, we evaluated the proliferative potential of these hepatocytes in immunodeficient, liver-injured mice [the urokinase-type plasminogen activator (uPA) transgenic NOD/Shi-scid IL2rγnull (NOG); uPA-NOG strain]. We succeeded in isolating viable hepatocytes from the livers of patients with BA who had various degrees of fibrosis. The isolated hepatocytes were intrasplenically transplanted into the livers of uPA-NOG mice. The hepatocytes of only 3 of the 9 BA patients secreted detectable amounts of human albumin in sera when they were transplanted into mice. However, human leukocyte antigen–positive hepatocyte colonies were detected in 7 of the 9 mice with hepatocyte transplants from patients with BA. We demonstrated that hepatocytes buried in the cirrhotic livers of patients with BA retained their proliferative potential. A liver that was reconstituted with hepatocytes from patients with BA was shown to be a functioning human liver

Additional Supporting Information may be found in the online version of this article.

**Abbreviations:** 5-CF, 5-carboxyfluorescein; 5-CFDA, 5(6)-carboxyfluorescein diacetate; αSMA, alpha smooth muscle actin; ABC, adenosine triphosphate–binding cassette; ALB, albumin; BA, biliary atresia; BC, bile canaliculus; CFDA, 5-carboxyfluorescein diacetate; CYP, cytochrome P450; GAPDH, glyceraldehyde-3-phosphate dehydrogenase; hALB, human albumin; H&E, hematoxylin and eosin; HIF, high intrinsic fluorescence; HLA, human leukocyte antigen; IF, intrinsic fluorescence; LT, liver transplantation; MRP2, multidrug resistance–associated protein 2; ND, not detected by an enzyme-linked immunosorbent assay; NGS, normal goat serum; NMS, normal mouse serum; NR1, nuclear receptor subfamily 1; NRS, normal rabbit serum; PELD, Pediatric End-Stage Liver Disease; PI, propidium iodide; SLC, solute carrier family; UGT, uridine diphosphate glucuronosyltransferase; uPA, urokinase-type plasminogen activator; VIM, vimentin.

The authors report no conflicts of interest.

Hiroshi Suemizu was the primary experimenter, performed all transplants, analyzed the liver-reconstituted mice, and wrote the article. Kazuaki Nakamura, Mureo Kasahara, Junichiro Fujimoto, and Akito Tanoue performed all isolations of human hepatocytes and managed all the clinical samples. Kenji Kawai provided all the tissue histology. Yuichiro Higuchi analyzed the liver-reconstituted mice. Masato Nakamura provided overall project planning and coordination.

This work was supported in part by Grants-in-Aid for Scientific Research to Hiroshi Suemizu (21240042) and Akito Tanoue (23300162) from the Japan Science and Technology Agency.

*These authors contributed equally to this work.

Address reprint requests to Hiroshi Suemizu, Ph.D., Biomedical Research Department, Central Institute for Experimental Animals, 3-25-12 Tonomachi, Kawasaki-Ku, Kawasaki, Kanagawa 210-0821, Japan. Telephone: +81-44-201-8530; FAX: +81-44-201-8541 or +81-44-201-8511; E-mail: suemizu@ciea.or.jp or nogmouse@ciea.or.jp

DOI 10.1002/lt.23916
View this article online at wileyonlinelibrary.com.
LIVER TRANSPLANTATION.DOI 10.1002/lt. *Published on behalf of the American Association for the Study of Liver Diseases*

with a drug-metabolizing enzyme gene expression pattern that was representative of mature human liver and biliary function, as ascertained by fluorescent dye excretion into the bile canaliculi. These results imply that removing the primary etiology via an earlier portoenterostomy may increase the quantity of functionally intact hepatocytes remaining in a cirrhotic liver and may contribute to improved outcomes. *Liver Transpl 20:1127-1137, 2014.* © 2014 AASLD.

Received January 2, 2014; accepted May 10, 2014.

Biliary atresia (BA), the most common pediatric cholestatic disease, is caused by the progressive fibro-obliterative obstruction of the extrahepatic and intrahepatic bile ducts within the first few weeks of life.[1,2] The current surgical treatment is sequential. In the first few weeks of life, a Kasai portoenterostomy is performed to bypass the obstructed extrahepatic bile ducts and restore the biliary flow.[3] Approximately 20% of all patients who undergo portoenterostomy during infancy survive into adulthood with their native liver.[2,4] In general, it is advantageous to perform portoenterostomy as early after birth as possible to optimize the chance of success.[5] Patients who fail to undergo portoenterostomy experience a gradual deterioration of liver function and develop progressive fibrosclerosis; after the initial successful establishment of bile flow, liver transplantation (LT) is the only treatment option. Although several etiologies of BA have been postulated, the precise pathogenesis of BA remains unknown. Some factors that might contribute to its development are genetic, infective, inflammatory, and toxic insults.[1] In most cases, BA is associated with an intensive inflammatory infiltrate; this knowledge led us to the conjecture that BA results from an infectious or autoimmune destruction of the bile ducts. For example, the infection of newborn mice with the Rhesus rotavirus results in a BA-like disease.[6-8] Meanwhile, hepatocytes from patients with BA have not been thought to be involved in the development of chronic obstructive cholestasis. We and other groups have developed mice with humanized livers in which the liver is reconstituted with human hepatocytes so that in vivo drug metabolism and liver regeneration can be studied.[9-11] Therefore, the aims of this study were to evaluate the in vivo proliferative potential and functional properties of hepatocytes buried in the cirrhotic livers of BA patients.

## MATERIALS AND METHODS

Specimens from the National Research Institute for Child Health and Development were collected in a standardized manner with the permission of the patients' families.

### Animals

All mouse studies were conducted in strict accordance with *Guide for the Care and Use of Laboratory Animals* from the Central Institute for Experimental Animals. All experimental protocols were approved by the animal care committee of the Central Institute for Experimental Animals (permit number 11029A). All surgeries were performed under isoflurane anesthesia, and all efforts were made to minimize animal suffering. All studies using mouse tissue with transplanted human cells were approved by the ethics and biosafety committee of the National Research Institute for Child Health and Development and the Central Institute for Experimental Animals. The urokinase-type plasminogen activator (uPA) transgenic NOD/Shi-scid IL2rγnull (NOG); uPA-NOG strain[11] was maintained through the breeding of a female uPA-NOG hemizygote with a male homozygote. The zygosity of the *uPA* transgene was presumed from the degree of liver damage, which was examined through the determination of the serum levels of alanine aminotransferase with a Fuji DRI-CHEM 7000 clinical biochemical analyzer (Fujifilm Corp., Tokyo, Japan). The uPA-NOG mice with serum alanine aminotransferase activity greater than 150 U/L were selected as homozygotes and were then used as transplant recipients.

### Isolation of Hepatocytes From the Livers of Patients With BA

The entire experimental protocol was approved by the ethics and research committee of the National Center for Child Health and Development. Written informed consent was obtained in each case. Except for the pieces of liver tissue that were used as pathological specimens, the enucleated diseased livers from the transplant recipients were discarded. The human hepatocytes used in this study were procured from liver tissue removed from BA patients who met the diagnostic criteria [Pediatric End-Stage Liver Disease (PELD) score[12] $\geq$ 6 points] for LT operations. The levels of fibrosis were categorized according to the following criteria: (I) mild (portal fibrous expansion to bridging fibrosis involving $\leq$50% of portal tracts), (II) moderate (bridging fibrosis involving >50% of portal tracts), and (III) severe (bridging fibrosis involving >50% of the portal tracts with nodular architectural changes).[13] Patient 141, who had grade III fibrosis and a PELD score of 0, had portopulmonary syndrome (intrapulmonary shunting). The shunt ratio, calculated with technetium-99m macroaggregated albumin (ALB) scintigraphy, was 16.8%, which indicated a relatively mild shunt. The hepatocytes were isolated from the resected liver tissue through the 2-step collagenase perfusion[14] of the liver samples, as described previously.[15] Hepatic parenchymal cells were isolated with low-speed centrifugation (50*g*). Cell numbers and viability were assessed with trypan blue exclusion.[16]

### Flow Cytometry Analysis

The hepatocytes were stained with 1 mg/mL propidium iodide (PI; Sigma-Aldrich Co. LLC, St. Louis, MO), which stains dead cells. The intensity of 502-nm fluorescence was measured as intrinsic fluorescence (IF). Flow cytometry data were collected with a FACSCanto analyzer and BD FACSDiva software (BD Biosciences, Franklin Lakes, NJ). The data were analyzed with the FlowJo program (Tree Star, Inc., Ashland, OR).

### Transplantation of Hepatocytes Into uPA-NOG Mice

Hepatocytes from patients with BA and commercially available cryopreserved human hepatocytes from a 4-year-old female (NHEPS, Lonza, Walkersville, MD) were used as donor cells. Young (8-week-old) male uPA-NOG mice were used as the recipients of the human hepatocytes. One million viable hepatocytes were injected intrasplenically via a Hamilton syringe with a 26-G needle. The successful engraftment of the human hepatocytes was evaluated through the measurement of the blood level of human albumin (hALB) with an hALB enzyme-linked immunosorbent assay quantitation kit (Bethyl Laboratories, Montgomery, TX) according to the manufacturer's protocol. The replacement index, which was the percentage of human donor hepatocytes in the recipient liver, was estimated according to the hALB concentration in chimeric mice.[17]

### Histology and Immunohistochemistry

The tissues were fixed with 4% (vol/vol) phosphate-buffered formalin (Mildform, Wako Pure Chemical Industries, Ltd., Osaka, Japan), and 5-μm paraffin-embedded sections were stained with Azan-Mallory staining reagents (Muto Pure Chemicals, Tokyo, Japan) to visualize the collagen and muscle fibers and with hematoxylin and eosin (H&E). Some sections were autoclaved for 10 minutes in a target retrieval solution [0.1 M citrate buffer (pH 6.0) and 1 mM ethylene diamine tetraacetic acid (pH 9.0)] and were then equilibrated at room temperature for 20 minutes. Monoclonal mouse anti–human leukocyte antigen (anti-HLA) class I (A-C) antibodies (clone EMR8-5, Hokudo, Sapporo, Japan; 1:2000),[18] polyclonal goat anti-human ALB antibodies (Bethyl Laboratories; 1:1500), polyclonal rabbit anti-cytochrome P450 3A4 (CYP3A4) antibodies (Abcam, Inc., Cambridge, MA; 1:500), monoclonal mouse anti-human Ki-67 antigen antibodies (clone MIB-1; Dako Denmark A/S; 1:50),[19] monoclonal mouse anti-human multidrug resistance–associated protein 2 (MRP2) antibodies (clone M2 III-6, Millipore, Billerica, MA; 1:100),[20] monoclonal rabbit anti-vimentin (anti-VIM) antibodies (clone SP20, Nichirei Bioscience, Tokyo, Japan; 1:1500),[21] and monoclonal rabbit anti–alpha smooth muscle actin (anti-αSMA) antibodies (clone 1A4, Leica Microsystems, Tokyo, Japan; 1:200)[22] were used as primary antibodies. Normal mouse serum (NMS), normal goat serum (NGS), and normal rabbit serum (NRS) were used as negative controls for immunostaining. For bright-field immunohistochemistry, the antibodies for mouse, goat, and rabbit immunoglobulin were visualized with amino acid polymer/peroxidase complex–labeled antibodies [Histofine Simple Stain MAX PO (M, G, and R), Nichirei Bioscience) and a Bond Polymer Refine Detection system (Leica Microsystems) with a diaminobenzidine substrate [Dojindo Laboratories, Kumamoto, Japan; 0.2 mg/mL 3,3′-diaminobenzidine tetrahydrochloride, 0.05 M tris(hydroxymethyl)-aminomethane with hydrochloric acid (pH 7.6), and 0.005% hydrogen peroxide]. The sections were counterstained with hematoxylin. Hepatic biliary obstructions were examined with Hall's bilirubin staining method.[23] The images were captured under an Axio Imager upright microscope (Carl Zeiss, Thornwood, NY) equipped with AxioCam HRm and AxioCam MRc5 charge-coupled device cameras (Carl Zeiss).

### Real-Time Quantitative Reverse-Transcription Polymerase Chain Reaction for Drug Metabolism–Related Gene Expression

The total cellular RNA was isolated from the livers with an RNeasy mini kit (Qiagen K.K.). Complementary DNA was synthesized with a high-capacity complementary DNA reverse transcription kit (Applied Biosystems, Foster City, CA) with random hexamers. TaqMan gene expression master mix and TaqMan gene expression assays (Applied Biosystems) were used for the real-time quantitative polymerase chain reactions; amplifications were performed with an ABI-Prism 7000 sequence detection system (Applied Biosystems). The comparative threshold cycle (Ct) method was used to determine the relative ratio of the gene expression for each gene, which was corrected with human glyceraldehyde-3-phosphate dehydrogenase (GAPDH) and referenced to the RNA extracted from donor hepatocytes. The TaqMan assay numbers are listed in Table 1.

### Biliary Excretion Test With 5(6)-Carboxyfluorescein Diacetate (5-CFDA)

The ester precursor of 5-carboxyfluorescein (5-CF), 5(6)-carboxyfluorescein diacetate (5-CFDA; 0.5 nmol; Sigma-Aldrich), was injected intravenously into the mouse tail vein. Ten minutes after the 5-CFDA injection, the liver was perfused with 50 nmol/L 5-CFDA for 3 minutes, and the liver was then embedded in an optimum cutting temperature (O.C.T.) compound (Sakura Finetek Japan Co., Ltd., Tokyo, Japan) and frozen in liquid nitrogen. Ten-micrometer-thick serial frozen sections were prepared and air-dried. The 5-CF fluorescent signals were captured with an Axio Imager upright microscope (Carl Zeiss) equipped with AxioCam HRm and AxioCam MRc5 charge-coupled device cameras (Carl Zeiss). After the microfluorographs were taken, the tissue sections were fixed and rehydrated sequentially in decreasing concentrations of ethanol and water, and this was followed by immunohistochemical staining for MRP2. Sections were counterstained with

TABLE 1. TaqMan Probe Information

| Gene Name | Gene Description | TaqMan Assay Number |
|---|---|---|
| *GAPDH* | Glyceraldehyde-3-phosphate dehydrogenase | Hs99999905_m1 |
| *ALB* | Albumin | Hs99999922_s1 |
| *CYP1A1* | Cytochrome P450, family 1, subfamily A, polypeptide 1 | Hs00153120_m1 |
| *CYP1A2* | Cytochrome P450, family 1, subfamily A, polypeptide 2 | Hs00167927_m1 |
| *CYP2A6* | Cytochrome P450, family 2, subfamily A, polypeptide 6 | Hs00868409_s1 |
| *CYP2B6* | Cytochrome P450, family 2, subfamily B, polypeptide 6 | Hs03044634_m1 |
| *CYP2C8* | Cytochrome P450, family 2, subfamily C, polypeptide 8 | Hs00258314_m1 |
| *CYP2C9* | Cytochrome P450, family 2, subfamily C, polypeptide 9 | Hs00426397_m1 |
| *CYP2C18* | Cytochrome P450, family 2, subfamily C, polypeptide 18 | Hs00426400_m1 |
| *CYP2C19* | Cytochrome P450, family 2, subfamily C, polypeptide 19 | Hs00426380_m1 |
| *CYP2D6* | Cytochrome P450, family 2, subfamily D, polypeptide 6 | Hs00164385_m1 |
| *CYP2E1* | Cytochrome P450, family 2, subfamily E, polypeptide 1 | Hs00559368_m1 |
| *CYP3A4* | Cytochrome P450, family 3, subfamily A, polypeptide 4 | Hs00430021_m1 |
| *CYP3A5* | Cytochrome P450, family 3, subfamily A, polypeptide 5 | Hs00241417_m1 |
| *UGT1A1* | Uridine diphosphate glucuronosyltransferase 1 family, polypeptide A1 | Hs02511055_s1 |
| *UGT2B15* | Uridine diphosphate glucuronosyltransferase 2 family, polypeptide B15 | Hs00870076_s1 |
| *ABCB1* | Adenosine triphosphate–binding cassette, subfamily B (MDR/TAP), member 1 | Hs00184500_m1 |
| *ABCB11* | Adenosine triphosphate–binding cassette, subfamily B (MDR/TAP), member 11 | Hs00184824_m1 |
| *ABCC2* | Adenosine triphosphate–binding cassette, subfamily C (CFTR/MRP), member 2 | Hs00166123_m1 |
| *ABCG2* | Adenosine triphosphate–binding cassette, subfamily G (WHITE), member 2 | Hs01053790_m1 |
| *SLC22A1* | Solute carrier family 22 (organic cation transporter), member 1 | Hs00427552_m1 |
| *SLC22A7* | Solute carrier family 22 (organic anion transporter), member 7 | Hs00198527_m1 |
| *SLC22A9* | Solute carrier family 22 (organic anion transporter), member 9 | Hs00971064_m1 |
| *NR1H4* | Nuclear receptor subfamily 1, group H, member 4 | Hs00231968_m1 |
| *NR1I2* | Nuclear receptor subfamily 1, group I, member 2 | Hs00243666_m1 |
| *NR1I3* | Nuclear receptor subfamily 1, group I, member 3 | Hs00901571_m1 |

hematoxylin. Another tissue section was fixed in 4% paraformaldehyde, and this was followed by immunofluorescent staining with monoclonal mouse anti-HLA class I (A-C) antibodies, a streptavidin/Texas Red–labeled secondary antibody (GE Healthcare Bio-Sciences), and H&E. Commercially available cryopreserved human hepatocytes (normal hepatocytes) and cells from the HCT 116 line (American Type Culture Collection, Manassas, VA), a human colorectal carcinoma cell line that easily engrafts and forms tumor cell colonies in NOG mouse livers,[24] were used as positive and negative controls for the formulation of the bile canaliculus (BC) network.

### Statistical Analyses

Group comparisons were performed with the Student *t* test for independent samples. *P* values less than 0.05 were considered significant (Prism 5, GraphPad Software, Inc., La Jolla, CA).

## RESULTS

### Engraftment of Hepatocytes From Patients With BA in uPA-NOG Mouse Livers

Using liver failure immunodeficient mouse models, we first evaluated the regenerative potential of the residual hepatocytes buried in the cirrhotic livers of patients with BA.[11] We succeeded in isolating viable hepatocytes from the livers of 9 BA patients with various degrees of fibrosclerosis (Table 2 and Fig. 1A). The typical gross morphology of a liver from a patient with BA is shown in Fig. 1B. There was no significant difference ($P = 0.45$) between the cell yields from patients with grade II fibrosis ($2.3 \pm 1.6$ million cells per gram of liver, $n = 3$) and patients with grade III fibrosis ($3.8 \pm 4.2$ million cells per gram of liver, $n = 6$; Fig. 1C). The cell viability was not significantly different ($P = 0.81$) between patients with grade II fibrosis ($76.7\% \pm 16.0\%$, $n = 3$) and patients with grade III fibrosis ($73.3\% \pm 23.0\%$, $n = 6$; Fig. 1D). The isolated hepatocytes were analyzed with flow cytometry (Fig. 1D). Because the IF signal of the hepatocytes from patients with BA was not increased in comparison with normal hepatocytes, it did not seem that bile accumulated within the hepatocytes, even in the patients with BA. The viable and engraftable hepatic parenchymal cells seemed to be present in the high intrinsic fluorescence (HIF) fraction; these cells had a very large cell mass and a complicated internal structure because the percentage of the HIF fraction correlated positively with the engraftability of the hepatocytes, which was based on the plasma concentration of hALB ($r^2 = 0.8784$; Fig. 1E, right). However, the cell viability did not show a direct correlation with the plasma concentration of hALB ($r^2 = 0.0515$; Fig. 1E, center) or the percentage of the HIF fraction ($r^2 = 0.0064$; Fig. 1E, left). The isolated hepatocytes were intrasplenically transplanted into uPA-NOG mice. Successful engraftment was evaluated in terms of the detection of hALB in the mouse serum

TABLE 2. Engraftment of Hepatocytes Derived From Patients With BA in uPA-NOG Mouse Livers

| Patient Information | | | | | Isolated Hepatocytes | | | Experimental Condition and Summarized Results | | | |
|---|---|---|---|---|---|---|---|---|---|---|---|
| | | | | | | | | | | Animals With Engraftment | |
| Number | Age | Sex | Fibrosis Level | PELD Score | Cells/g of Liver | Viability (%) | HIF (%) | Condition* | Cell Dose (Cells/Mouse) | HLA-Positive Colony [n/N (%)]† | hALB [n/N (μg/mL)] |
| 80 | 10 months | Female | II | 20 | $1.2 \times 10^6$ | 66 | 9.0 | A | $1.0 \times 10^6$ | 5/5 (100) | 5/5 (230-875) |
| | | | | | | | | B | $1.0 \times 10^6$ | 4/4 (100) | 1/4 (280) |
| | | | | | | | | C | $1.0 \times 10^6$ | 4/4 (100) | 1/4 (38) |
| 86 | 7 months | Female | II | 35 | $1.5 \times 10^6$ | 95 | 4.8 | A | $1.0 \times 10^6$ | 2/2 (100) | 1/2 (35) |
| | | | | | | | | B | $1.0 \times 10^6$ | 2/4 (50) | 1/4 (105) |
| 153 | 8 months | Male | II | 9 | $4.1 \times 10^6$ | 69 | 1.3 | B | $1.0 \times 10^6$ | 2/3 (67) | 0/3 (ND) |
| 105 | 5 months | Female | III | 13 | $1.2 \times 10^7$ | 83 | 8.5 | B | $1.0 \times 10^6$ | 4/4 (100) | 4/4 (49-294) |
| 133 | 6 months | Female | III | 15 | $6.9 \times 10^4$ | 33 | 9.2 | B | $2.0 \times 10^5$ | 0/1 (0) | 0/1 (ND) |
| 141 | 12 years | Female | III | 0 | $3.0 \times 10^6$ | 93 | 4.8 | B | $1.0 \times 10^6$ | 1/1 (100) | 0/1 (ND) |
| 149 | 8 months | Female | III | 14 | $3.4 \times 10^6$ | 67 | 0.8 | B | $1.2 \times 10^6$ | 3/3 (100) | 0/3 (ND) |
| 151 | 5 months | Female | III | 10 | $1.4 \times 10^6$ | 69 | 5.0 | B | $1.0 \times 10^6$ | 3/4 (75) | 0/4 (ND) |
| 154 | 6 months | Female | III | 14 | $3.1 \times 10^6$ | 95 | 4.2 | B | $1.0 \times 10^6$ | 0/1 (0) | 0/1 (ND) |
| 77 | 32 years | Male | Normal | — | $2.0 \times 10^6$ | 88 | 25.5 | C | $1.0 \times 10^6$ | 5/5 (100) | 5/5 (35-1516) |

*The conditions were as follows: (A) fresh hepatocytes (within the first 6 hours after isolation), (B) chilled hepatocytes (stored at 4°C for more than 16 hours and up to 24 hours), and (C) cryopreserved hepatocytes.
†Hepatocyte colonies that contained more than 20 HLA-positive cells in the cross-sections.

and the appearance of HLA-positive hepatocyte colonies in the liver tissue (Fig. 1F). Although detectable amounts of secreted hALB were found only in the sera of mice that had received hepatocyte transplants from 3 of the 9 BA patients, HLA-positive hepatocyte colonies were detected as a result of 7 of the 9 hepatocyte transplants from patients with BA.

The expression of drug-metabolizing enzymes, a marker of a fully matured liver, was analyzed with real-time quantitative polymerase chain reaction. Livers reconstituted with hepatocytes from 2 different patients with BA (patients 80 and 105) and commercially available cryopreserved hepatocytes (NHEPS) were then examined. The relative gene expression profiles of hepatocytes from patients with BA were similar to those of NHEPS hepatocytes (Fig. 1G). The expression levels of most of the genes were higher in the reconstituted livers versus the donor hepatocytes (Fig. 1H).

Next, we examined the expression of ALB, a major functional marker of biosynthesis in the liver, via immunohistochemical staining with human-specific antibodies in hepatocytes originating from patients with BA (Fig. 2A, top and middle). This hepatic lineage marker protein was expressed within the human hepatocyte colonies in the reconstituted-liver mice at levels comparable to those of the liver reconstituted with cryopreserved normal hepatocytes (patient 77; Fig. 2A, bottom). The expression of CYP3A4, which is the main drug-metabolizing enzyme found in the liver, was also observed within the colonies consisting of both hepatocytes from patients with BA (Fig. 2A, top and middle) and normal hepatocytes (Fig. 2A, bottom), but it did not show the zonal distribution observed in the fully reconstituted uPA-NOG liver with NHEPS hepatocytes (Fig. 2B). Most human hepatocytes originating from the patients with BA were present as small foci that appeared to grow by clonal expansion within the uPA-NOG mouse livers. This growth was quite similar to that of normal hepatocytes from patient 77. In addition, immunohistochemical nuclear staining of serial sections of the mouse livers with an antibody (MIB-1) against the human Ki-67 antigen[25,26] revealed that the proliferative potential of the hepatocytes from the patients with BA was preserved, as evidenced by the nuclear staining of the hepatocytes located at the edges of human hepatocyte colonies (Fig. 2A, top and middle). NGS, NRS, and NMS (nonimmune), which corresponded to the host animals in which anti-ALB, anti-CYP3A4, and anti–Ki-67 antibodies, respectively, were prepared, did not react with either human or mouse hepatocytes (Fig. 2C). The hepatocyte colonies derived from the patients with BA were not stained by Azan-Mallory staining (Fig. 2A, top and middle).

## Functional Integrity of Partially Humanized Livers

We confirmed the expression of MRP2 proteins on the plasma membranes of hepatocytes in both the livers of patients with BA and the partially humanized livers repopulated with hepatocytes from patients with BA

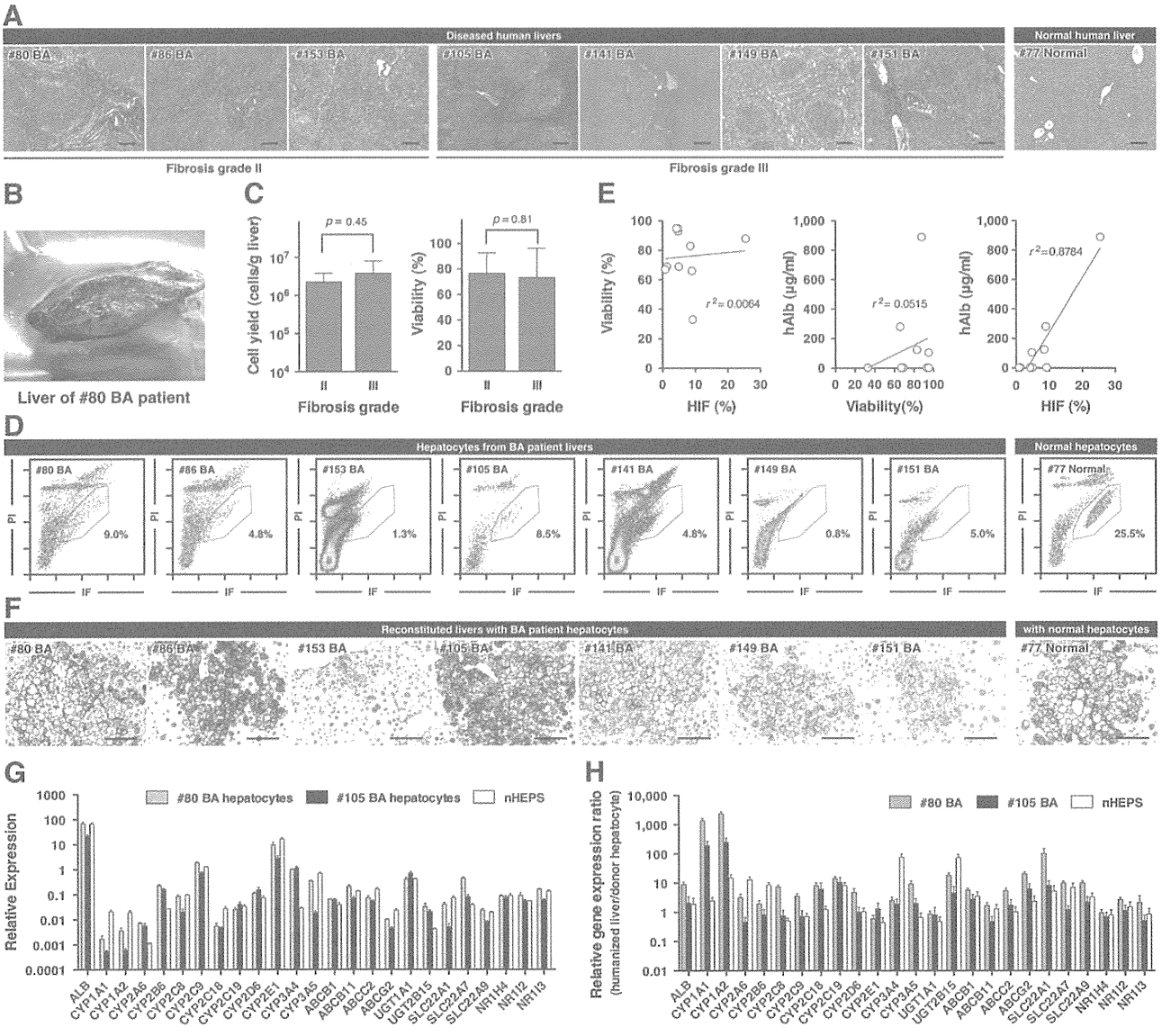


Figure 1. Engraftment of hepatocytes from BA patients in uPA-NOG mouse livers. (A) Azan-Mallory staining of 7 individual liver biopsy samples from BA patients and a healthy donor (normal). The scale bars represent 200 μm. (B) Gross morphology of the liver from BA patient 80. (C) Comparison of the cell yields and viability with grade II hepatic fibrosis and grade III hepatic fibrosis. (D) Isolated hepatocytes were analyzed with flow cytometry. Each HIF fraction is surrounded by a magenta border. (E) Correlation analyses of the cell viability, the HIF fraction percentage, and the hALB plasma concentration. (F) The engraftment of hepatocytes isolated from the BA patients and the healthy donors was confirmed with anti-human HLA staining. The scale bars represent 50 μm. (G) The relative expression levels of 24 human drug metabolism–related messenger RNAs in hepatocytes from BA patients and NHEPS hepatocytes were corrected with GAPDH. (H) The relative ratio of the gene expression for each reconstituted liver was referenced to the RNA extracted from the donor hepatocytes.

(Fig. 3A,B,). The cholestasis, visualized with Hall's bilirubin staining, was observed in many BCs in the livers of patients with BA (Fig. 3A, right). In contrast, the colonies repopulated with hepatocytes from patients with BA within the host mouse livers did not accumulate bile within their BCs (Fig. 3B). Azan-Mallory staining and VIM and αSMA antibody staining revealed fibrosis in the livers of patients with BA (Fig. 3C), but no fibrosis was observed within the colony repopulated with hepatocytes from patients with BA (Fig. 3D). We wondered whether these hepatocytes could reconstitute the functionally integrated BC network within the host mouse liver; therefore, we assessed the transporter function within the colonies of hepatocytes from patients with BA with 5-CFDA, a fluorescent marker used to visualize biliary excretion into BCs. After it is administered, 5-CFDA enters hepatocytes and is metabolized into 5-CF. This compound is excreted into BCs through the organic anion transporter MRP2.[27] Within the first 15 minutes after the administration of 5-CFDA, the hepatocytes from patients with BA in the uPA-NOG mice excreted 5-CF into the BCs, and it formed honeycomb networks surrounding individual hepatocytes (Fig. 4, top). This

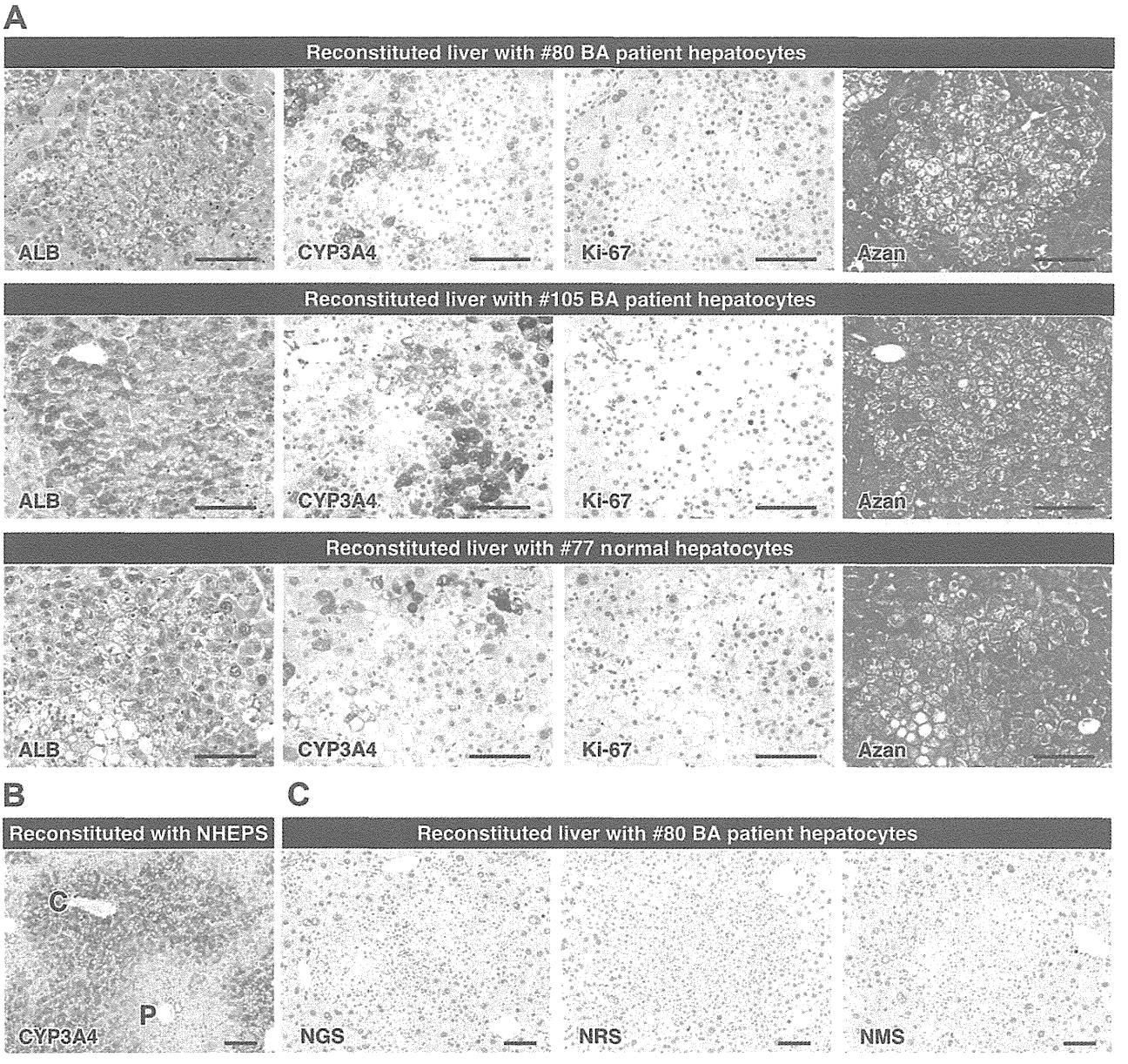


Figure 2. Immunohistochemistry of uPA-NOG mouse livers engrafted with BA patient hepatocytes. (A) Sections were stained for hALB, human CYP3A4, and human Ki-67 antigen; Azan-Mallory staining was also used. The scale bars represent 100 μm. (B) Immunohistochemical staining for CYP3A4 in a fully reconstituted uPA-NOG liver with NHEPS hepatocytes. The scale bar represents 100 μm. (C) Negative controls for immunostaining: NGS, NRS, and NMS. The scale bars represent 100 μm.

process was also observed in the colonies of NHEPS hepatocytes (Fig. 4, middle) but not in the HCT 116 colorectal tumors (Fig. 4, bottom). The typical BC network was detectable in the human hepatocyte conglomerates, as visualized by anti-MRP2, HLA antibodies, and H&E staining (Fig. 4). These results suggest that the intrahepatic bile duct system within the colonies reconstituted with hepatocytes from patients with BA must be nondefective.

## DISCUSSION

BA is the most common reason for LT in children worldwide. The aim of this study was to evaluate regenerative medicine as a possible alternative to LT for treating BA. We succeeded in isolating viable hepatocytes from the livers of patients with BA so that we could evaluate the regenerative potential in vivo with a liver failure mouse model.[11] Recently, Gramignoli et al.[28] reported the successful isolation of hepatocytes from people with a number of different metabolic and other liver diseases (n = 35). The purpose of their study was to evaluate hepatocytes from individuals with metabolic disease for use in cell therapy via hepatocyte transplantation. Although they performed hepatocyte isolation in patients with BA (n = 7), those cells would not be recommended for clinical transplants because of concerns about cell yields, viability,

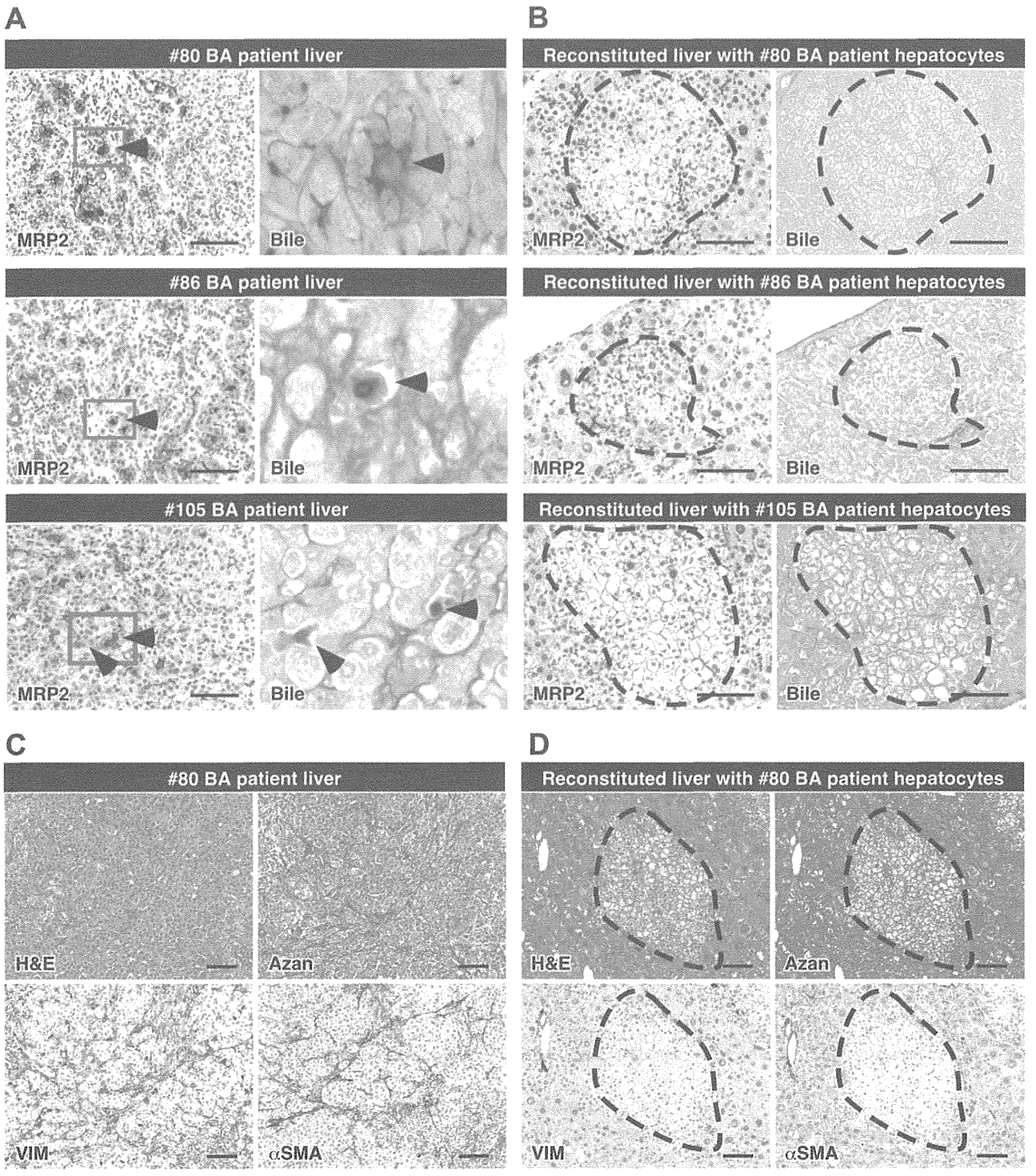


Figure 3. Detection of biliary obstructions and hepatic fibrosis. (A) Immunohistochemical staining for MRP2 protein in livers from patients with BA (patients 80, 86, and 105; left). Enlarged views of the boxed areas are shown with Hall's bilirubin staining (right). Bile stained with Hall's method appears green (arrowheads). (B) Immunohistochemical staining for MRP2 protein (left) and Hall's bilirubin staining (right) in uPA-NOG mouse livers engrafted with hepatocytes from BA patients (patients 80, 86, and 105). The dotted areas indicate the repopulated human liver. (C) H&E and Azan-Mallory staining and immunohistochemical staining for VIM and αSMA in the liver from a BA patient (patient 80). (D) H&E and Azan-Mallory staining and immunohistochemical staining for VIM and αSMA in a uPA-NOG mouse liver engrafted with hepatocytes from a BA patient (patient 80). The dotted areas indicate the repopulated human liver. The scale bars represent 100 μm.